An Analysis of the Contributions of Line-End Vortices, Gravity Waves, and Environmental Flow to Mesoscale Convective System Rear Inflow and Stratiform Region Structure in Numerical Simulations

Dillon Blount[1], Clark Evans[1,3], Rebecca Adams-Selin[2], Hannah Vagasky[2]

[1]University of Wisconsin-Milwaukee, [2]Atmospheric and Environmental Research, [3]NOAA/OAR Global Systems Laboratory

Introduction

- Both line-end vortices and gravity waves are hypothesized to contribute to MCS rear-to-front flow, which is important for governing MCS morphology.
- Line-end vortices can enhance the rear-to-front flow though a non-divergent wind associated with cyclonic vertical vorticity.
- Convectively generated gravity waves are associated with horizontal pressure perturbations that can modify the horizontal flow.

Main Hypothesis

Gravity waves are a leading contributor to the rear-to-front flow that varies over time with gravity wave modifications, line-end vortices, and environmental flow. These contributions will vary over time depending on the strength of each component.

Methods

- We perform wind decomposition (Oertel and Schemm 2021) to determine flow contributions from the line-end vortex versus the total wind field.

Non-divergent wind (vorticity) **Irrotational Wind** (divergence)

$$u_{\psi_\Omega}(x,y) = -\frac{\partial \psi_\Omega}{\partial y} = \frac{1}{2\pi}\int_\Omega \zeta(x',y')\frac{-(y-y')}{r^2}\mathrm{d}x'\mathrm{d}y' \qquad v_{\psi_\Omega}(x,y) = \frac{\partial \psi_\Omega}{\partial x} = \frac{1}{2\pi}\int_\Omega \zeta(x',y')\frac{(x-x')}{r^2}\mathrm{d}x'\mathrm{d}y'$$

$$u_{\chi_\Omega}(x,y) = \frac{\partial \chi_\Omega}{\partial x} = \frac{1}{2\pi}\int_\Omega \delta(x',y')\frac{(x-x')}{r^2}\mathrm{d}x'\mathrm{d}y' \qquad v_{\chi_\Omega}(x,y) = \frac{\partial \chi_\Omega}{\partial y} = \frac{1}{2\pi}\int_\Omega \delta(x',y')\frac{(y-y')}{r^2}\mathrm{d}x'\mathrm{d}y'$$

- The total pressure gradient driving the rear inflow can be divided into (Weisman 1993; Grim et al. 2009):

$$\delta P_T = \delta P_B + \delta P_I + \delta P_V + \delta P_S$$

Total = Buoyancy + Irrotational + Vorticity + Synoptic/Environmental — matches previous studies

our hypothesized breakdown

$$\delta P_T = \delta P_B + \delta P_W + \delta P_I + \delta P_V + \delta P_S$$

Total = Buoyancy + Waves* + Irrotational + Vorticity + Synoptic/Environmental

*Low-frequency gravity wave response

Gravity wave contributions will be assessed by subtracting the horizontal wind change from before and after wave passage.

WRF Simulations

- ERA5 Reanalysis and HRRR are used for initial and lateral boundary conditions for the outer domains.
- A one-way nest-down process is used to get to the innermost domain.
- Case #1: 20 May 2011 (MC3E)
  - 3 km: 30 hours, MYNN2, NSSL 2-mom
  - 1 km: 20 hours, MYNN2, NSSL 2-mom
  - 1/3 km: 11 hours, no PBL, NSSL 2-mom
- Case # 2: 17 June 2015 (PECAN)
  - 3 km: 12 hours, MYNN2, NSSL 2-mom
  - 1 km: 12 hours, MYNN2, NSSL 2-mom
  - 1/3 km: 11 hours, no PBL, NSSL 2-mom

Verification

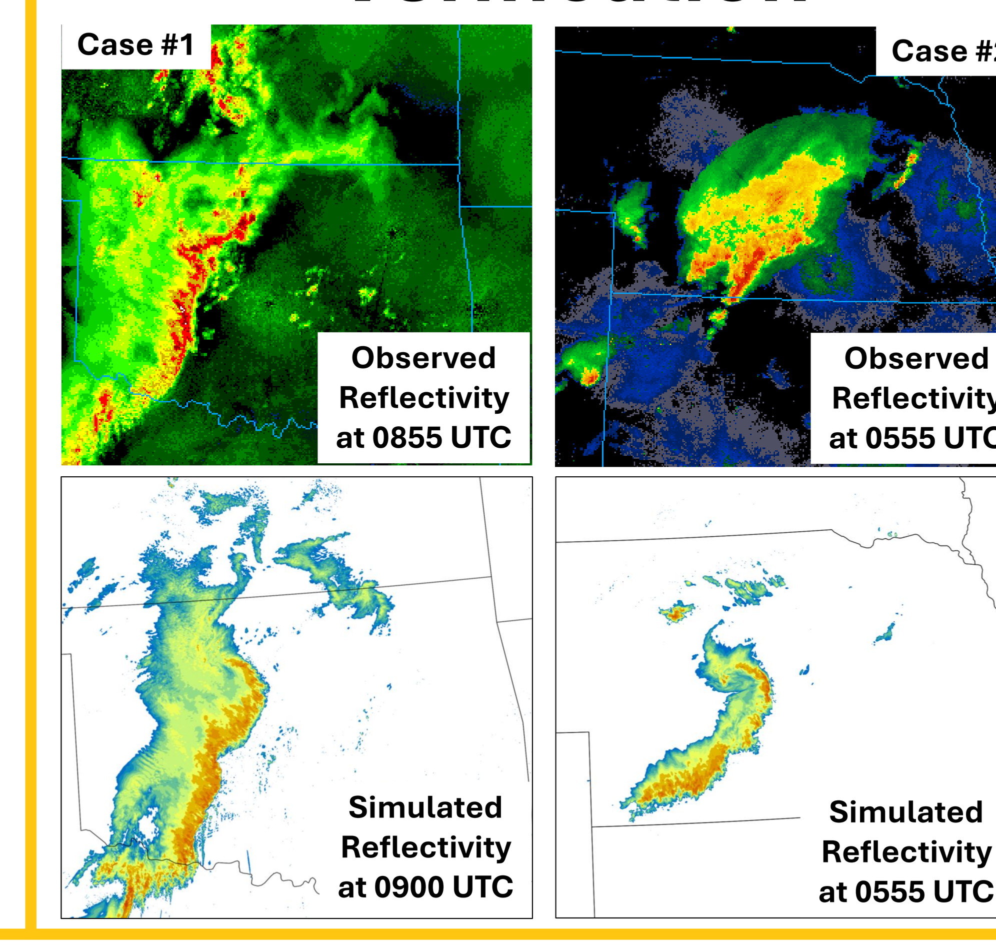

Case #1 Results

1000 UTC Storm Relative Line Perpendicular Wind Vertical Cross-Section

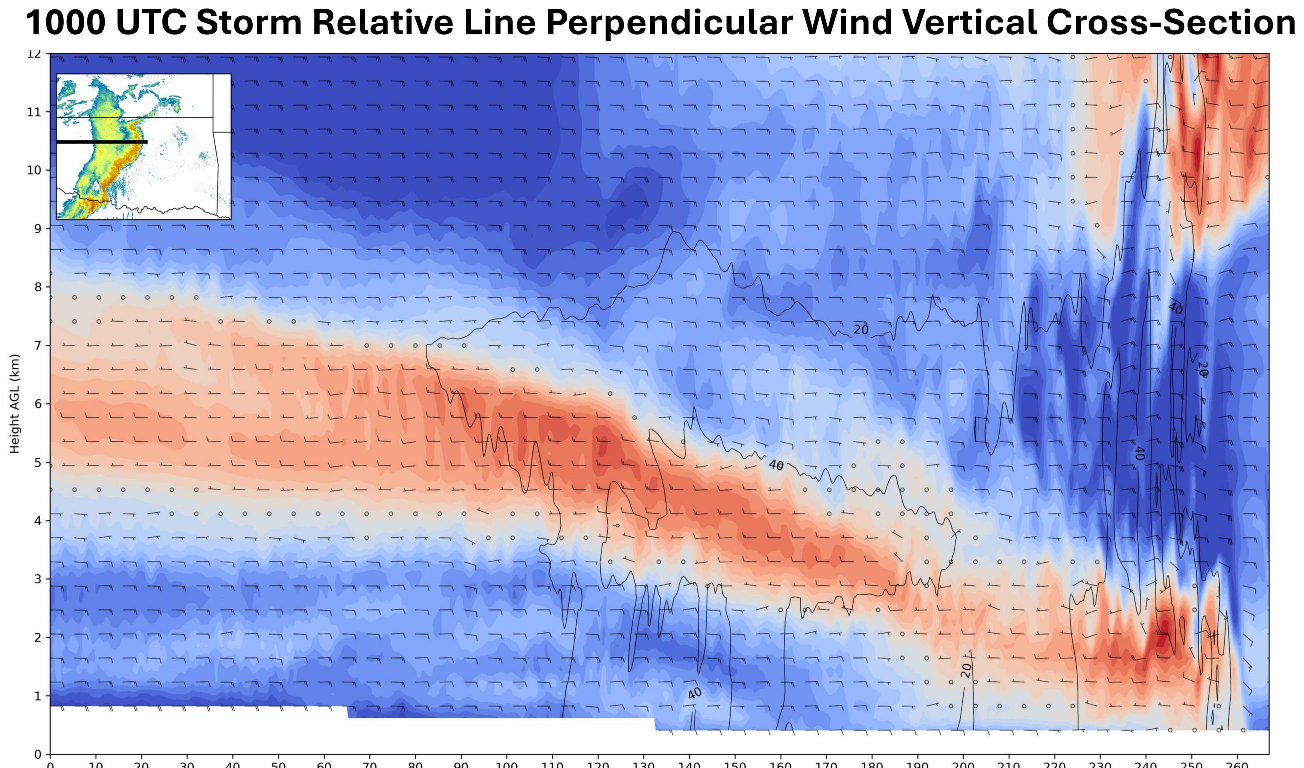

Hovmöller Plot of 14 km AGL Vertical Motion 0830-1200 UTC on 2011 May 20

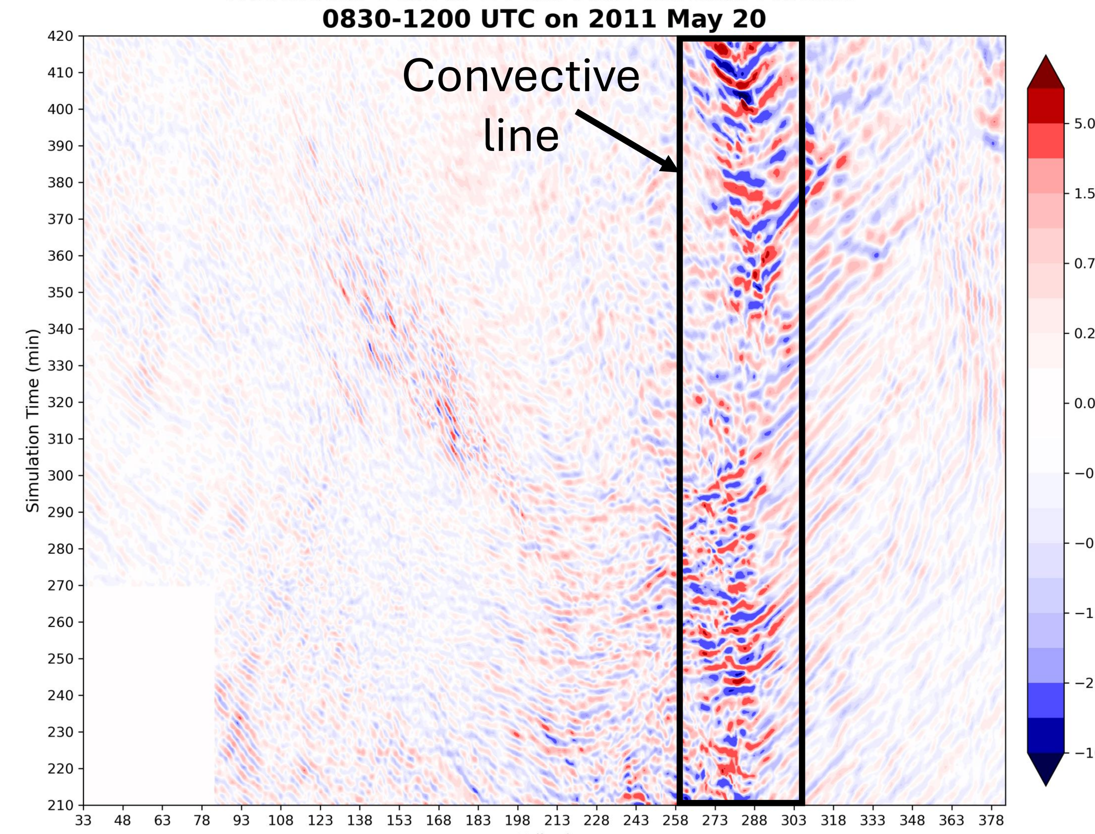

3 km AGL Non-Divergent Wind (orange) and Total Wind (grey) at 0900 UTC on 20 May 2011

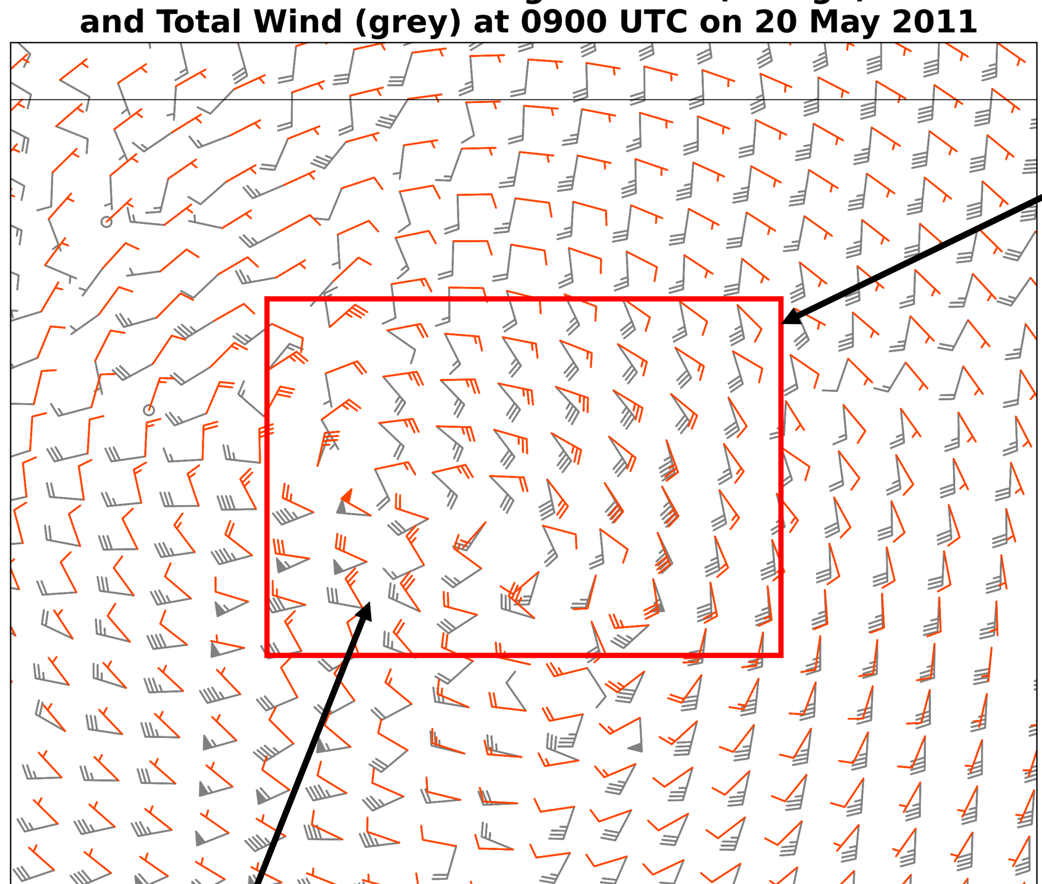

All vorticity outside of the red box is set to zero

Large contributions (80-100%) to the total wind due to vorticity south of the northern line-end vortex

Contributions extend well outside of the vorticity area. However, these contributions are small

Power Spectrum of 14.0 km Vertical Velocity 0830-1200 UTC on 2011 May 20

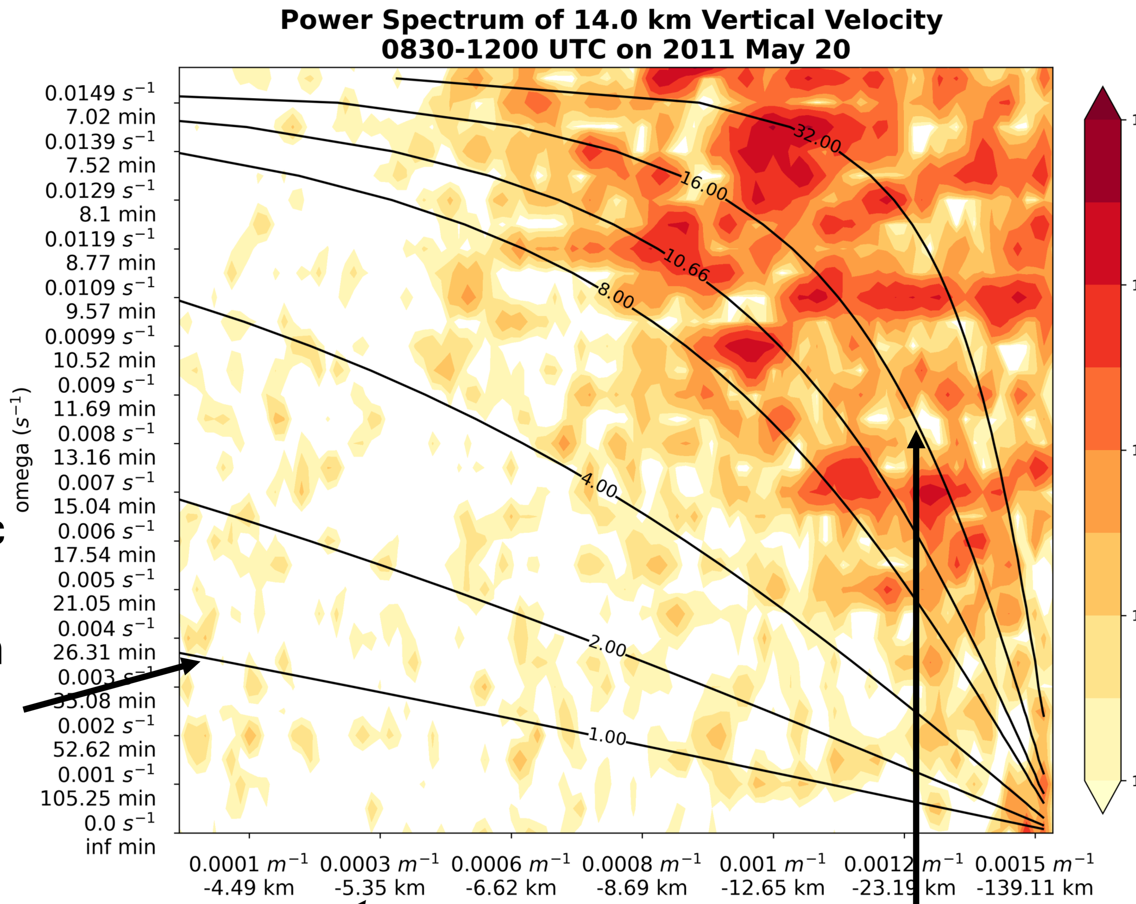

Nonhydrostatic dispersion relations which can be related to wave type (i.e., 32 is a n=1 wave)

Negative wavenumber/wavelength indicates rearward moving waves

Most power in the upper right quadrant which is consistent with low-frequency waves

Case #2 Results

This case shows full system evolution better than Case #1

0500 UTC Storm Relative Line Perpendicular Wind Vertical Cross-Section

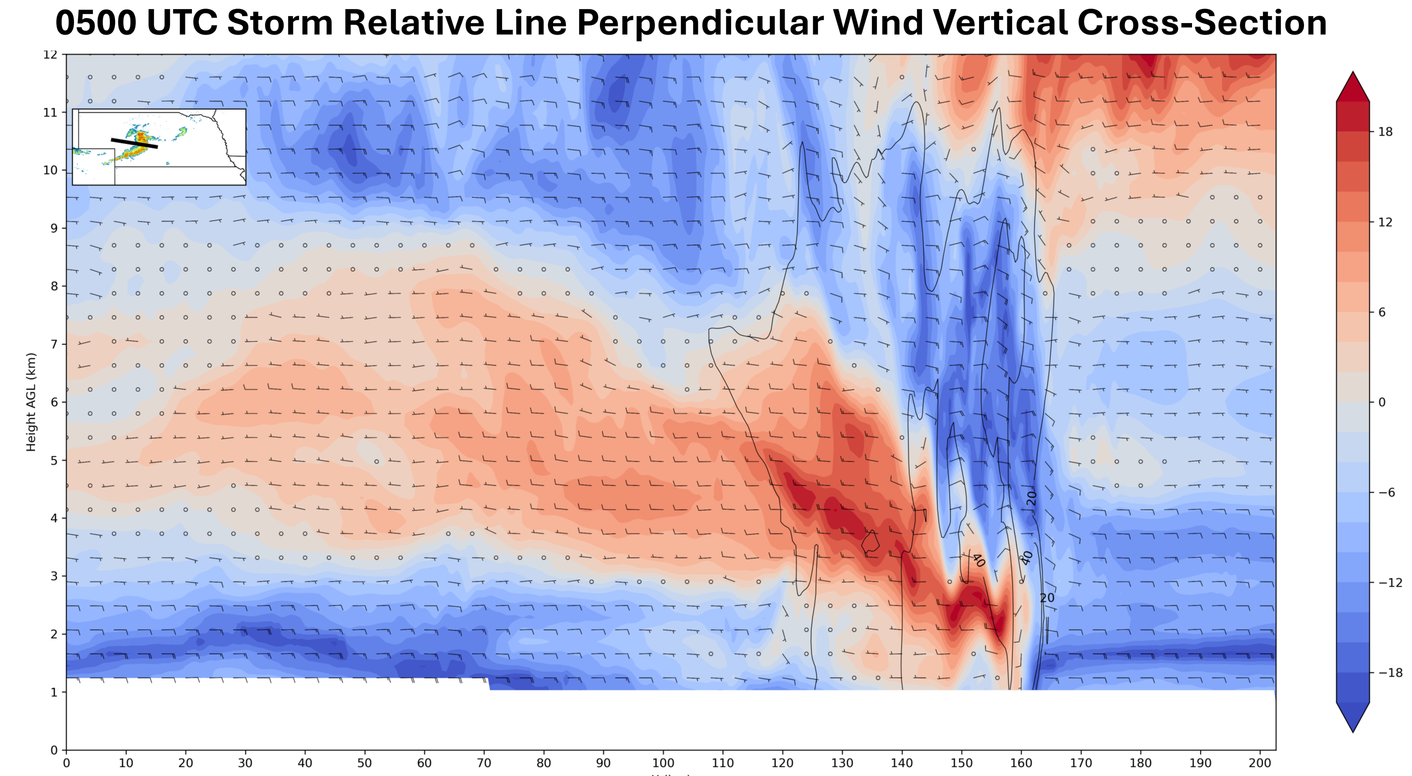

Vertical motions in the Hovmöller plot shows more vertical wave-like features in this case than in Case #1

Hovmöller Plot of 14 km AGL Vertical Motion 0400-0800 UTC on 2015 Jun 17

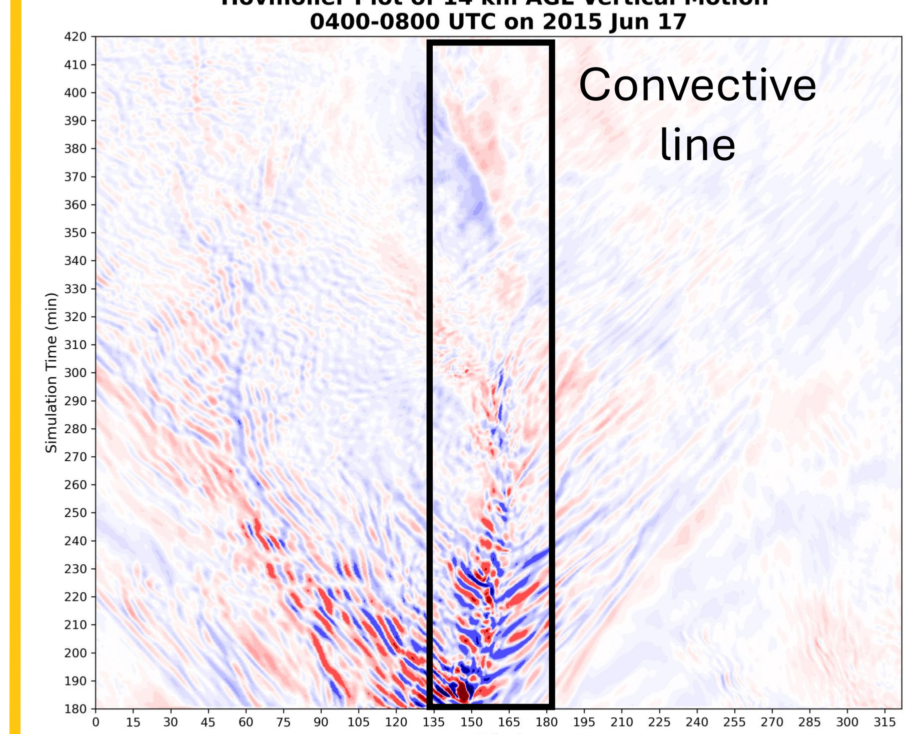

Power is concentrated in the 04-06 UTC for this case with little power observed after 06 UTC

Power aligns with contours indicating n=1 and n=2 gravity waves

Power Spectrum of 14 km Vertical Velocity 0400-0800 UTC on 2015 Jun 17

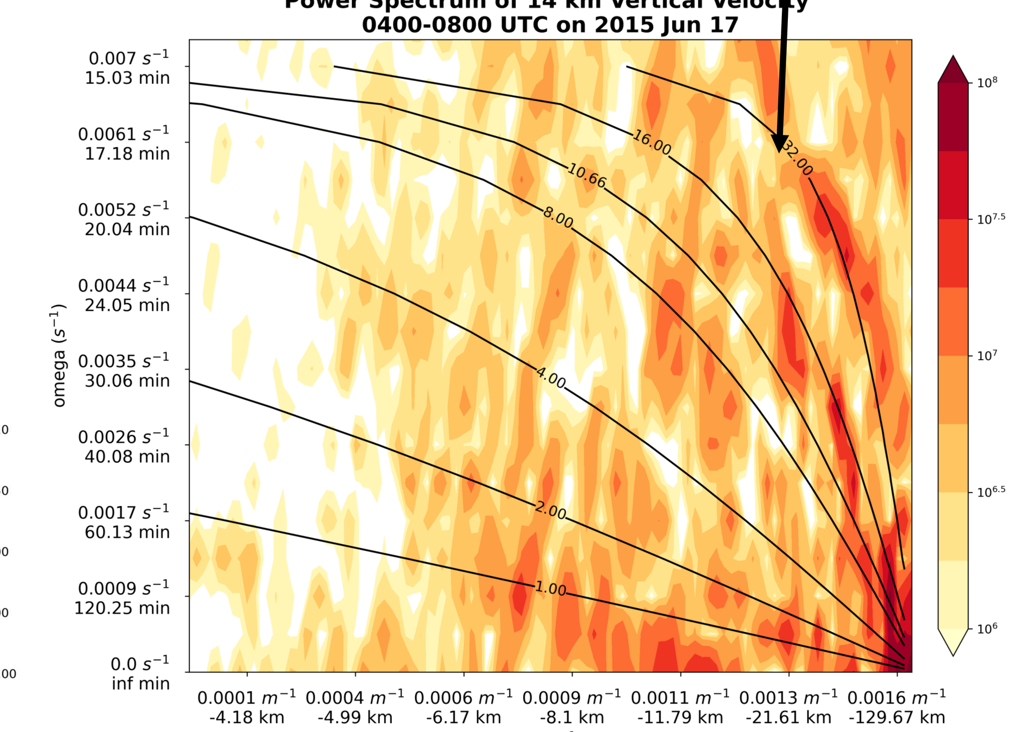

Conclusions

- Case #1 simulation verifies much better than Case #2 versus reflectivity observations
- Vorticity due to the northern line-end vortex of Case #1 is contributing a substantial percentage of the total wind
- Spectral analysis supports the presence of low-frequency gravity waves in numerical simulations of both cases
- Future work is to continue assessing the wind decomposition for both cases through time, assess the horizontal wind change before and after gravity wave passage, and assess the environmental flow contribution

Contact: dvblount@uwm.edu

Funding provided by ASR Award DE-SC0023057